ARTICLES

Spin-integrated and spin-resolved photoemission study of Fe chalcogenides

K. Shimada,* T. Mizokawa, K. Mamiya, T. Saitoh, and A. Fujimori
Department of Physics, University of Tokyo, Bunkyo-ku, Tokyo 113, Japan

K. Ono,† A. Kakizaki, and T. Ishii
Institute for Solid State Physics, University of Tokyo, Tokyo 106, Japan

M. Shirai
Department of Material Physics, Osaka University, Toyonaka, Osaka 560, Japan

T. Kamimura
Department of Physics, Tohoku University, Sendai 980-77, Japan
(Received 19 February 1997)

The electronic structures of the antiferromagnetic semiconductor FeS and ferrimagnetic metals Fe_7S_8 and Fe_7Se_8 have been studied by spin-integrated and spin-resolved photoemission spectroscopy and inverse-photoemission spectroscopy. The overall Fe $3d$ bandwidth in the photoemission spectra is 25–30 % narrower than the density of states (DOS) predicted by first-principles band-structure calculations and is accompanied by an intense tail on the high-binding-energy side, indicating the correlated nature of electrons in the Fe $3d$ band. Deviation from the band DOS is more significant in Fe_7S_8 than in Fe_7Se_8, and in the minority-spin spectra than in the majority-spin spectra. Cluster-model calculation for FeS has shown satellite structures at high binding energies, but the calculated spectral line shape is not in good agreement with experiment compared to the band DOS. By introducing a self-energy correction to the band DOS, we could explain the narrowing of the overall Fe $3d$ bandwidth and the high-binding-energy tail shape but not for the unusual broadening of the Fe $3d$ band within ~ 1 eV of the Fermi level. [S0163-1829(98)02415-1]

I. INTRODUCTION

It is well known that electron correlation is important in $3d$ transition-metal oxides and d electrons in these compounds have tendencies to be localized in many cases. d electrons in transition-metal chalcogenides generally have more itinerant character than those in corresponding oxides because covalency between the transition-metal d orbitals and the anion p orbitals becomes stronger as the atomic number of anion increases from O to S to Se to Te. In the present paper, we have investigated the electronic structures of some iron chalcogenides, FeS, Fe_7S_8, and Fe_7Se_8, using photoemission and inverse-photoemission spectroscopy. FeS (troilite) and Fe_7S_8 (pyrrhotite) are among the most common iron compounds in earth. The electrical and magnetic properties of these compounds have been studied so far, but their electronic structures have not been well understood. We shall compare the observed spectra with a localized-electron model, namely, the configuration-interaction (CI) cluster model and with an itinerant electron model, namely, band-structure calculations. We shall clarify the effects of electron correlation with the use of cluster-model calculation and self-energy correction to the density of state (DOS) derived from the band-structure calculations.

FeS is antiferromagnetic below the Néel temperature of $T_N = 593$–598 K.[1,2] Above $T_\alpha = 420$ K,[2,3] FeS is a metal with the NiAs-type crystal structure, but becomes an insulator with a narrow band gap of 0.04 eV below T_α.[2,3] This transition, known as the α transition, is accompanied by a small displacement of the Fe and S atoms from the regular NiAs-type structure, and leads to the so-called ''troilite structure.''[4,5] According to a neutron diffraction study, the temperature dependence of the magnetic reflection intensity near the Néel temperature can be well explained by the Brillouin function of the $S=2$ (d^6) local moment.[5] The magnitude of the hyperfine field also shows the same temperature dependence.[2]

Fe_7S_8 and Fe_7Se_8 are ferrimagnetic metals with Néel temperatures of $T_N = 578$ and 423–460 K, respectively.[1] The crystal structures of Fe_7S_8 and Fe_7Se_8 are derived from the NiAs-type one by introducing ordered Fe vacancies.[6–9] The metal-full and metal-deficient layers are alternatively stacked along the c direction. The compounds are referred to as $2c$, $3c$, and $4c$ structures according to the unit-cell periodicity along the c axis.[8,9] The easy axis of Fe_7Se_8 lies within the c plane above $T = 220$ K ($3c$ Fe_7Se_8) or 130 K ($4c$ Fe_7Se_8) but is off the c plane below it.[10–13] The same behavior has been observed for Fe_7S_8.[1] The temperature dependence of the easy magnetization axes has been well explained using a spin Hamiltonian.[1] In such a localized-electron model, the metal-full layer consists of Fe^{2+} ions (with the ordered moment of $4\mu_B$) and the metal-deficient layers consist of both Fe^{2+} and Fe^{3+} ions (with the ordered moments of $4\mu_B$ and $5\mu_B$, respectively). According to neutron diffraction studies,[13–16] however, the magnitudes of the magnetic moments are smaller than $4\mu_B$ (Fe^{2+}) and $5\mu_B$ (Fe^{3+}). The observed magnetic moments of Fe_7S_8 in the metal-full and the metal-deficient layers are $3.0\mu_B$ and $3.5\mu_B$,

respectively.[14] The magnetic moments of Fe_7Se_8 have not been accurately determined but they are also significantly smaller than $4–5\mu_B$ (Refs. 13 and 15) and their site dependence is small,[13] indicating the itinerant nature of the Fe $3d$ electrons. Also, the ionic electron configurations cannot explain the result of Mössbauer studies.[17–20] On the other hand, the effective magnetic moment of Fe_7Se_8 derived from the paramagnetic susceptibility, $\sim 5.5\mu_B$, agrees well with the ionic model.[21]

Recently, first-principles band-structure calculations using the local-spin-density approximation (LSDA) have been performed for FeS (Ref. 22), Fe_7S_8 (Ref. 23), and Fe_7Se_8 (Ref. 24) and their electronic structures have been discussed from the itinerant-electron point of view. According to the calculations, the ground state of FeS is an antiferromagnetic semimetal with a magnetic moment of $3.0\mu_B$,[22] which is smaller than the ionic value of $4\mu_B$.[5] As for Fe_7S_8, the calculated magnetic moment in the metal-full layer ($3.2\mu_B$ and $2.9\mu_B$) and that in the metal-deficient layer ($-3.0\mu_B$) show reasonable agreement with the neutron diffraction study.[14] The calculated magnetic moments for Fe_7Se_8 ($3.1\mu_B$, $2.8\mu_B$, and $-3.0\mu_B$) are smaller than those for Fe_7S_8.[23,24] It is also indicated that the calculated optical conductivity spectrum of Fe_7Se_8 (Ref. 24) agrees well with the experimental spectrum.[25] In the band-structure calculations, the $1c$ structure has been assumed for Fe_7S_8 and Fe_7Se_8, considering that the electronic structure would not be sensitive to the periodicity of vacancy ordering. On the other hand, according to the calculation for Fe_7Se_8, the electronic specific-heat coefficient is $\gamma = 3.1$ mJ/K^2 atomic mol,[24] which is smaller than the experimental values, 8 and 4.4 mJ/K^2 atomic mol (for $4c$ and $3c$ Fe_7Se_8, respectively) (Refs. 26 and 27). For Fe_7S_8, too, the calculated value $\gamma = 3.1$ mJ/K^2 atomic mol (Ref. 23) is significantly smaller than the experimental values, 4.9 and 7.8 mJ/K^2 atomic mol (for $4c$ and $3c$ Fe_7S_8, respectively).[27] This implies a mass enhancement of conduction electrons due to electron correlation.

II. EXPERIMENT

We have studied polycrystals of FeS, Fe_7S_8, $3c$ Fe_7Se_8, and single crystals of $4c$ Fe_7Se_8. We used $3c$ Fe_7Se_8 for x-ray photoemission spectroscopy (XPS) and resonant photoemission spectroscopy, and $4c$ Fe_7Se_8 for high-resolution ultraviolet photoemission spectroscopy, inverse-photoemission spectroscopy [bremsstrahlung isochromat spectroscopy (BIS)], and spin-resolved photoemission spectroscopy (SRPES). We found no detectable differences in the line shape between the $3c$ and $4c$ compounds. The samples were synthesized by the Bridgman method, which are described in detail elsewhere.[21]

A 0.4-GeV electron storage ring at the Synchrotron Radiation Laboratory, Institute for Solid State Physics, University of Tokyo was used as an excitation source for resonant photoemission studies. A double-pass cylindrical-mirror analyzer (DCMA) was used for energy analysis. Samples were mounted on a liquid nitrogen cryostat. In order to obtain clean surfaces, they were scraped *in situ* with a diamond file. The overall energy resolution was 0.4–0.5 eV for $h\nu = 40–100$ eV. The base pressure was 6×10^{-11} Torr. Binding energies were referenced to the Fermi edge of freshly evaporated Au. Spectra taken at different photon energies were normalized to the photon flux determined by the total yield of Au. The spectra were also corrected for the transmission of the DCMA.

As for XPS measurements, we used a spectrometer equipped with a Mg x-ray source (Mg $K\alpha$: $h\nu = 1253.6$ eV) and a DCMA. The energy resolution was ~ 1 eV. The satellites of the Mg $K\alpha$ x ray were numerically subtracted. High-resolution ultraviolet photoemission measurements were made using a spectrometer equipped with a He discharge lamp (He I: $h\nu = 21.2$ eV and He II: $h\nu = 40.8$ eV) and a 150 mm-radius hemispherical analyzer. The samples were mounted on a closed-cycle He refrigerator and cooled down to 25–30 K. The energy resolution was estimated from the Fermi edge of Au evaporated on the samples and found to be 25–30 meV for He I and 80–90 meV for He II. BIS measurements were made using a SiO_2 crystal monochromator to detect photons of $h\nu = 1486.6$ eV. The energy calibration was made using the Fermi edge of Au evaporated on the samples. The total energy resolution was ~ 0.8 eV. The samples were mounted on a liquid nitrogen cryostat and were cooled during the measurements.

The SRPES measurements were performed on the $4c$ Fe_7Se_8 single crystals and the Fe_7S_8 polycrystals. The measurements were done at the Revolver undulator beamline BL-19A of the Photon Factory, National Laboratory for High Energy Physics.[28] A 100-kV Mott detector[29] was used for spin analysis. The samples were cut into a disk of 3 mm diameter and 0.5 mm thickness and mounted on a liquid-He flow cryostat and cooled to 30–35 K. Clean surfaces were obtained by fracturing and afterwards by scraping *in situ* with a diamond file. The energy resolution was 0.5 eV for $h\nu = 65$ eV. Prior to the SRPES measurements, we measured the hysteresis curves of the Fe_7S_8 and Fe_7Se_8 samples using a SQUID magnetometer. The saturation magnetization was attained under an external magnetic field of 0.5 T, but the residual magnetization was 20–60 % and 25% of the saturation magnetization for Fe_7S_8 and Fe_7Se_8, respectively, at ~ 30 K. In order to magnetize the samples *in situ*, we used a coil made of a 2 mm$^{\phi}$ Cu wire connected to a condenser bank for current supply. A pulsed magnetic field of >1 T with a duration of ~ 0.1 msec was produced by the coil, which sufficiently exceeds the coersive force of the present samples. During the photoemission measurements, we magnetized the sample every hour and reversed the magnetization direction. According to the SQUID measurements, the residual magnetization remained unchanged for more than 1 h. We repeated the SRPES measurements changing the direction of the residual magnetization by changing the external magnetic field. We took an average over the photoemission spectra taken for the opposite residual magnetization and calculate the asymmetry A. One can deduce the spin polarization (P) by $P = A/S_{\text{eff}}$, where S_{eff} is a Sherman function ($S_{\text{eff}} = 0.23$ for the present detector). Using the spin polarization and the spin-integrated total intensity I one can derive the intensity of majority- and minority-spin emission $I_\uparrow$ and $I_\downarrow$, by $I_\uparrow = I(1+P/f)/2$ and $I_\downarrow = I(1-P/f)/2$. Here, f (<1) is the residual magnetization divided by the saturation magnetization to account for the incomplete magnetization of the sample. It should be noted that if there were no spin-polarization effects, the majority- and minority-spin spectra would be identical.

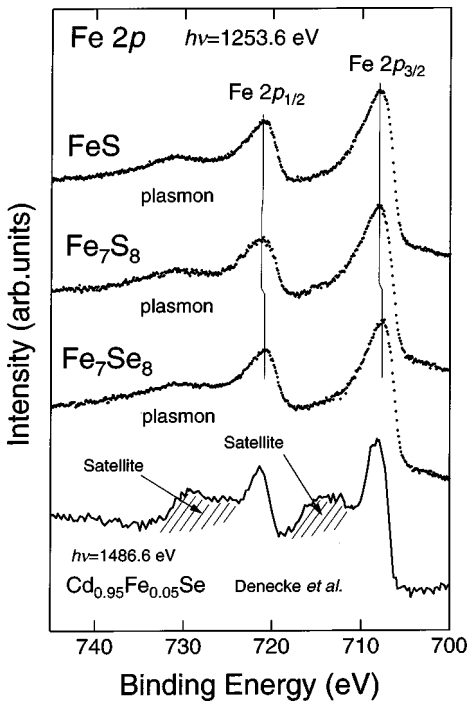

FIG. 1. Fe $2p$ core-level spectra of FeS, Fe_7S_8, Fe_7Se_8, and $Cd_{0.95}Fe_{0.05}Se$ (Ref. 30).

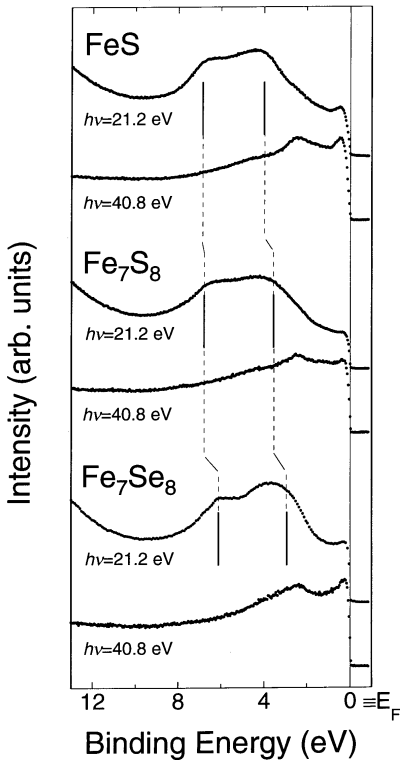

FIG. 2. Valence-band photoemission spectra of FeS, Fe_7S_8, and Fe_7Se_8. Vertical bars indicate the peak positions determined from second derivatives.

III. RESULTS

The Fe $2p$ core-level XPS spectra of FeS, Fe_7S_8, Fe_7Se_8, and $Cd_{0.95}Fe_{0.05}Se$ are shown in Fig. 1. The broad peak located at binding energy $E_B \sim 730$ eV is largely due to a plasmon satellite accompanying the Fe $2p_{3/2}$ peak, judging from the plasmon satellites for the S and Se core-level spectra. While clear charge-transfer satellites were seen in the Fe $2p$ spectrum of $Cd_{1-x}Fe_xSe$,[30] in which the Fe $3d$ electrons are localized and the electronic states are well described by the CI cluster model,[30,31] the Fe $2p$ spectra of FeS, Fe_7S_8, and Fe_7Se_8 show only the main peaks with a high-binding-energy tail. However, the existence of broad satellites within the tail cannot be excluded.

Figure 2 shows the valence-band photoemission spectra of FeS, Fe_7S_8, and Fe_7Se_8. The calculated photoionization cross sections of Fe $3d$, S $3p$, and Se $4p$ are comparable [(Fe $3d$)/(S $3p$) = 1.12 and (Fe $3d$)/(Se $4p$) = 0.60] for He I excitation ($h\nu = 21.2$ eV) whereas the cross section of Fe $3d$ is larger by a factor of ~ 15 than those of S $3p$ and Se $4p$ for He II excitation ($h\nu = 40.8$ eV).[32] Because the structures at $E_B = 3$–4 and 6–7 eV are strong for $h\nu = 21.2$ eV, they are assigned to S $3p$ or Se $4p$ states. In going from FeS to Fe_7S_8, the structure at $E_B = 6$–7 eV is slightly shifted towards E_F. The shifts are consistent with the decrease in the filling of the Fe $3d$ band because the formal valence of Fe in Fe_7S_8 ($Fe^{+2.28}$) is higher than that (Fe^{2+}) in FeS.

Figure 3 shows photoemission spectra taken in the Fe $3p \rightarrow 3d$ core-absorption region. In the figure, we also show difference spectra between on and off resonance. In the $h\nu = 56.9-52.5$ eV difference spectrum of FeS, one can identify peaks at $E_B \sim$ 10, 5, and 2.6 eV. The broad peak at $E_B \sim 10$ eV is the Fe MVV Auger peak. The peak at $E_B \sim 2.6$ eV is resonantly enhanced at $h\nu \sim 57$ eV. In the $h\nu = 54.8-52.5$ eV difference spectrum, the intensity of the ~ 2.6 eV peak becomes weak and the peak just below the Fermi level (E_F), $E_B \sim 0.3$ eV, becomes clearer, as in the case of $Cd_{1-x}Fe_xSe$.[30] We can identify a broad peak at $E_B \sim 5$ eV, which becomes a broad tail accompanying the main Fe $3d$ band at $h\nu = 40$ eV.

One can recognize the same situation in Fe_7S_8, namely, a broad structure at $E_B \sim 5$ eV although the enhancement at $E_B \sim 2.6$ eV in the difference spectra becomes weaker. The different resonance behaviors between FeS and Fe_7S_8 indicate the different degrees of the itinerant character of the Fe $3d$ electrons. In the Fe $2p$ core-level spectra and the valence-band spectra of the iron sulfides taken away from the Fe $3p \rightarrow 3d$ resonance, the satellite structures are not clearly identified or are embedded in the tail of the main structure.

As for Fe_7Se_8, the valence-band spectrum is enhanced as a whole, and the $h\nu = 57-52$ eV difference spectrum resembles the $h\nu = 49$ eV spectrum, which represents the Fe $3d$ states. The satellite structure is not clear as in the iron sulfides. These observations indicate that electrons in the Fe $3d$ band of Fe_7Se_8 are more itinerant than the iron sulfides.

Figure 4 shows the constant-initial-state (CIS) spectra of FeS, Fe_7S_8, and Fe_7Se_8 for $E_B = 0.2$–0.3 eV and 2.3–2.6 eV. The CIS spectra show rather simple Fano-type profiles,[33] similar to the CIS spectra of other metallic systems. The CIS spectra for smaller E_B tend to be of antiresonance type while those for larger E_B tend to be of resonance type. If we compare Fe_7S_8 and Fe_7Se_8, the deduced q parameter of the Fano line shape is larger for Fe_7S_8 ($E_B = 0.3$ eV: $q = 0.5$; $E_B = 2.6$ eV: $q = 1.0$) than for Fe_7Se_8 ($E_B = 0.2$ eV: $q = 0.1$; $E_B = 2.3$ eV: $q = 0.75$). This indicates that the super-Coster-Kronig contribution is larger[33] and the probability of the di-

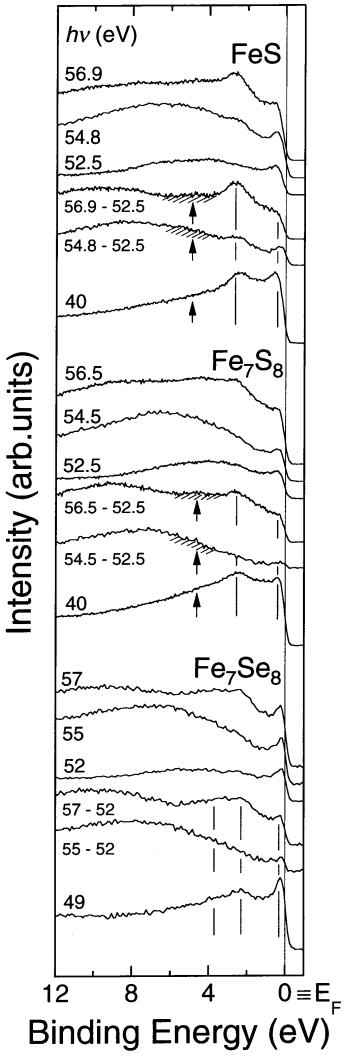

FIG. 3. Photoemission spectra of FeS, Fe_7S_8, and Fe_7Se_8 in the Fe $3p \rightarrow 3d$ core absorption region. Dots represent difference spectra. Shaded regions (marked with arrows) imply the existence of satellites.

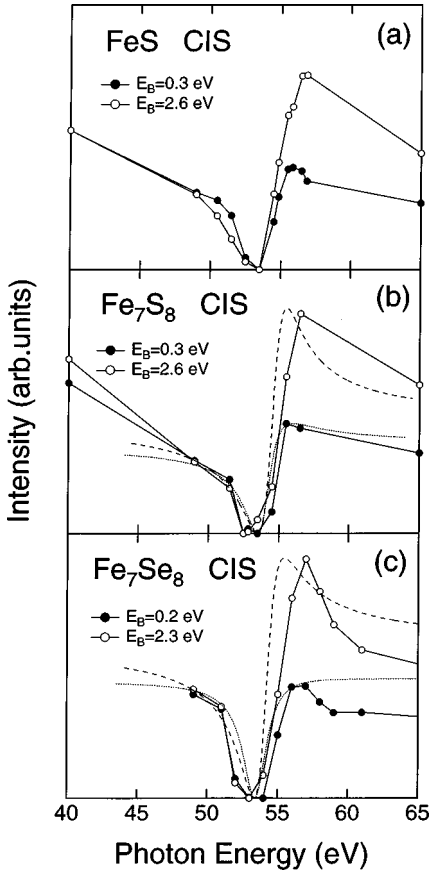

FIG. 4. Constant-initial-state (CIS) spectra of FeS, Fe_7S_8, and Fe_7Se_8. Dashed lines are fitted Fano profiles.

rect recombination of excited electrons is higher in Fe_7S_8 than in Fe_7Se_8. The higher probability of the direct recombination means a more localized nature of excited electrons in the Fe $3d$ band. In more localized systems such as $Cd_{1-x}Fe_xSe$, one can see two peaks in the CIS spectra corresponding to the ^5D, ^5F, and ^5P states of the intermediate $3p^5 3d^6$ multiplet.[30] Such a multiple-peak structure is not obvious in the present case.

Figure 5 shows high-resolution photoemission spectra near E_F taken with $h\nu = 21.2$ eV. The intensity at E_F of FeS is low, reflecting the insulating state. Because the photoionization cross section of Fe $3d$ and that of S $3p$ are almost the same for He I, we have normalized the He I spectra of FeS and Fe_7S_8 so that the integrated spectral intensity is proportional to the number of electrons per sulfur atom in the valence band. Near E_F ($E_B = 0$–0.15 eV), the photoemission intensity of Fe_7S_8 is higher than that of FeS, reflecting the metallic conductivity in Fe_7S_8. However, the photoemission intensity steeply decreases toward E_F (compared with the Fermi edge of Au) even in metallic Fe_7S_8 and Fe_7Se_8. This tendency is more significant for Fe_7S_8 than for Fe_7Se_8.

IV. DISCUSSION

A. Evolution of the electronic structure from FeS to Fe_7S_8

Changes in the spectra in going from the antiferromagnetic insulator FeS to the ferrimagnetic metal Fe_7S_8 can be viewed in two ways. One is to start from the band picture ignoring electron correlation. As the Fe vacancies are introduced, the filling of the Fe $3d$ band decreases as a result of the large number of removed electrons compared to the number of removed Fe $3d$ states. The other picture is to consider hole doping into the Mott insulator FeS, where Fe is formally divalent with the high-spin d^6 configuration. The 12.5% Fe vacancies in Fe_7S_8 lead to a doping of ~ 0.3 holes per Fe into the Fe $3d$ band of FeS. As a result, the lower Hubbard band is shifted toward E_F and spectral weight is transferred from below E_F to above it and fill the band gap region of FeS. This spectral weight transfer will be accompanied by additional spectral weight transfer towards higher binding energies separated from E_F by the intra-atomic Coulomb energy U of Fe $3d$.

The photoemission and BIS spectra of FeS and Fe_7S_8 are shown in Fig. 6. The difference between FeS and Fe_7S_8 cannot be explained by a simple rigid band model. We have to explicitly consider the effect of the Fe vacancies on the band structure if we use the itinerant band model. On the other hand, from the hole-doped Mott insulator picture, we can indeed see the behavior expected for the hole-doped Mott insulator as schematically shown in the inset of Fig. 6. Namely, the intensity at E_F (particularly that just above E_F,

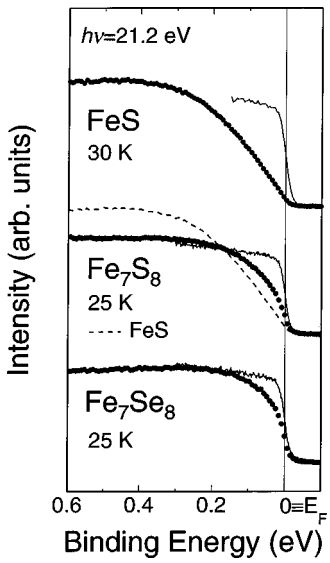

FIG. 5. High-resolution photoemission spectra near E_F of FeS, Fe_7S_8, and Fe_7Se_8. The dashed line represents photoemission spectrum of FeS and the solid lines represent photoemission spectra of Au evaporated on the samples.

so-called ''in-gap'' spectral weight, i.e., $d^5 \rightarrow d^6$) is increased in going from FeS to Fe_7S_8 together with a decrease in the peak intensity at $E \sim -0.3$ eV ($d^6 \rightarrow d^6\underline{L}$ spectral weight, where $\underline{L}$ denotes a ligand hole) and at $E \sim +1$ eV ($d^6 \rightarrow d^7$ spectral weight, that is, the upper Hubbard band). On the other hand, there is an increase at $E \sim -4$ eV (assigned to $d^5 \rightarrow d^4$ spectral weight, the lower Hubbard band). From this we evaluate $U \sim 4$ eV.

B. Comparison with band-structure calculation

In Fig. 7, we compare the photoemission and BIS spectra of FeS, Fe_7S_8, and Fe_7Se_8 with the DOS derived from the band-structure calculation.[22–24] The band DOS has been

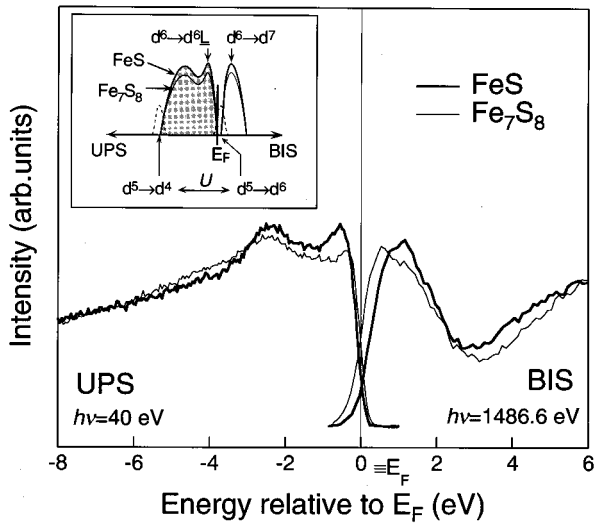

FIG. 6. Photoemission and BIS spectra of FeS and Fe_7S_8. The inset shows a schematic view of the hole-doped Mott insulator. Thicker and thinner lines represent FeS and Fe_7S_8, respectively. Dashed lines represent new states created by iron vacancies.

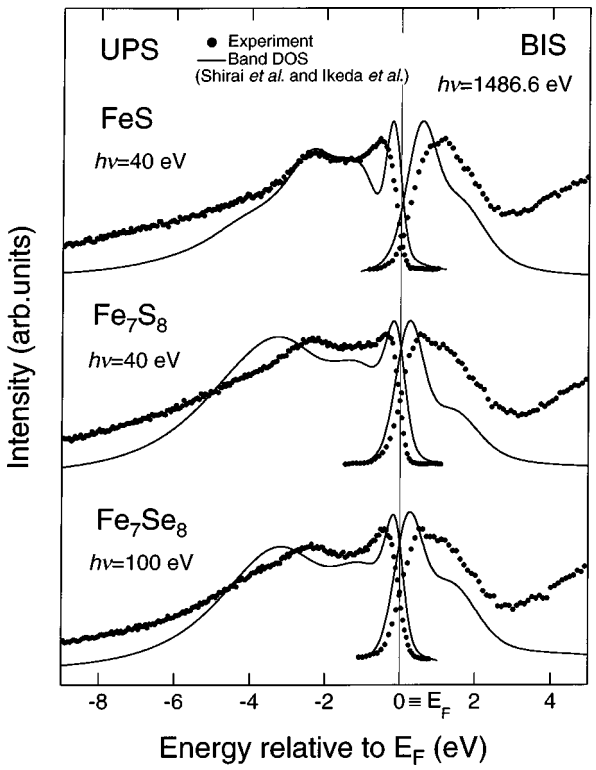

FIG. 7. Photoemission and BIS spectra of FeS, Fe_7S_8, and Fe_7Se_8 compared with broadened band DOS (Refs. 23 and 24). Integral backgrounds have been subtracted from the photoemission spectra.

broadened with the experimental energy resolution and the lifetime broadening, which linearly increases with energy from E_F. The BIS spectra of Fe_7S_8 and Fe_7Se_8 are almost identical to each other. There is a peak at $E \sim +1$ eV for FeS and at $E \sim +1.5$ eV for Fe_7S_8 and Fe_7Se_8. According to the band-structure calculations, the broad peak at $E \sim -2.5$ eV comes from the Fe $3d$-$t_{2g\uparrow}$ band, the sharp peak at $E \sim -0.3$ eV from the Fe $3d$-$e_{g\uparrow}$ and Fe $3d$-$t_{2g\downarrow}$ bands, and $E \sim +1$–1.5 eV mainly from Fe $3d$-$e_{g\downarrow}$ band.[22–24]

As for FeS, since the band gap is not opened in the band-structure calculation,[22] we have shifted the valence and conduction bands so as to give the band gap of 0.04 eV, which was obtained from the electrical conductivity and thermoelectric power measurements.[3] Since FeS is a p-type semiconductor, we have aligned the top of the calculated occupied states at E_F. It should be noted that the band-structure calculation for FeS was done for the ideal NiAs-type crystal structure[22] although Fe atoms in FeS are displaced from the regular position below $T_\alpha = 411$ K.[4,5]

Figure 7 also shows that the overall Fe $3d$ bandwidth in the experimental spectra is 25–30 % narrower than that in the calculated DOS for Fe_7S_8 and Fe_7Se_8. On the other hand, all the observed spectra have an intense tail at higher binding energies, $E_B > 5$ eV, irrespective of background and plasmon-satellite subtraction. Contrary to the overall narrowing of the Fe $3d$ band, the measured peak near E_F ($E \sim -0.3$ eV) is broader than the calculated one. The near E_F peak in the BIS spectra of Fe_7S_8 and Fe_7Se_8 is also broader in experiment than in the calculation. This is more clearly seen in the high-resolution photoemission spectra shown in Fig. 8, where one can see that the broadening near E_F is more sig-

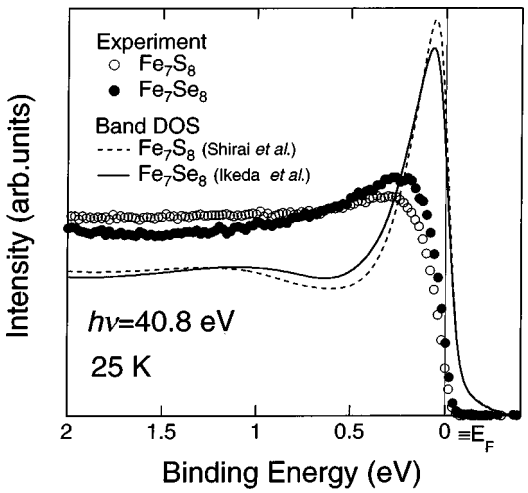

FIG. 8. High-resolution photoemission spectra of Fe_7S_8 and Fe_7Se_8 near E_F compared with broadened band DOS (Refs. 23 and 24). The theoretical and experimental spectra have been normalized to the total integrated intensities.

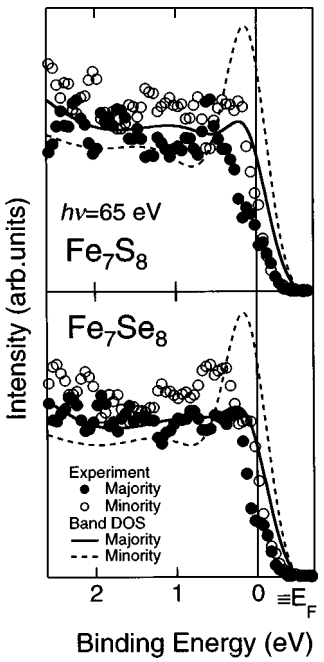

FIG. 9. Spin-resolved photoemission spectra of Fe_7S_8 and Fe_7Se_8 near E_F compared with the broadened band DOS (Refs. 23 and 24). The closed and open circles represent the majority- and minority-spin spectra, respectively, and the solid and dashed curves the corresponding DOS.

nificant in Fe_7S_8 than in Fe_7Se_8. Larger deviation from the calculated DOS in Fe_7S_8 than in Fe_7Se_8 indicates the stronger electron correlation effects in Fe_7S_8. This is consistent with the observation of the satellite feature in the resonant photoemission measurements of Fe_7S_8 but not of Fe_7Se_8.

Here, it is noticed in Fig. 7 that the difference between the calculated and observed Fe $3d$ bandwidths is more significant for Fe_7S_8 than in FeS although the localized nature of Fe $3d$ electrons in FeS is stronger than in Fe_7S_8 as described above. This is probably due to the underestimation of the magnetic moment in the band-structure calculation of FeS: The calculated magnetic moment on the Fe atom, $3.0\mu_B$,[22] is indeed smaller than the value from neutron diffraction, $4\mu_B$.[5]

The SRPES photoemission spectra of Fe_7S_8 and Fe_7Se_8 near E_F are compared with the calculated spin-up and spin-down DOS in Fig. 9. Although the observed spin polarization ($\sim 5\%$) was small due to small residual magnetization ($\sim 20\%$), the spin-polarization spectra show structures near E_F. The SRPES spectra shown in Fig. 9 are those expected for fully magnetized samples obtained by correcting for the incomplete magnetization. The experimental minority-spin intensity is dominant near E_F, in agreement with the calculation. However, the peak just below E_F is significantly broader than that of the theoretical curve, especially for Fe_7S_8. While the calculated majority-spin (or minority-spin) density of states of Fe_7S_8 and Fe_7Se_8 are very similar, the observed spectra are different between these compounds. A peak structure is absent in the observed minority-spin spectrum of Fe_7S_8 while it is obvious in that of Fe_7Se_8. It indicates larger deviation from the calculated DOS in Fe_7S_8 than in Fe_7Se_8, consistent with the results of the satellite structure of iron sulfides observed in the resonant photoemission measurements and the hole-doped Mott insulator picture. The broadening effect is more significant for the minority-spin spectrum than that of the majority-spin spectrum. It suggests that the broadening in the observed spin-integrated spectra near E_F (Fig. 8) is a result of spin-dependent spectral weight redistribution, especially in the minority-spin spectra. The present result is opposite to the case of Ni metal, in which the majority-spin band is more strongly affected by electron correlation than the minority-spin band.[34] Different band structures and band fillings between the two systems may be responsible for the different behaviors of the SRPES spectra.

C. Comparison with configuration-interaction cluster-model calculations

In order to clarify the effect of electron correlation on the photoemission spectra, we have performed a CI cluster-model calculation[35–37] for the antiferromagnetic insulator FeS. We have used an octahedral $(FeS_6)^{10-}$ cluster and assumed that the Fe^{2+} ion is in the high-spin d^6 ($S=2$) configuration. The initial state $|\Phi_i\rangle$ and the final state $|\Phi_f\rangle$ of the photoemission process have the forms of $|\Phi_i\rangle = a_6|d^6\rangle + a_7|d^7\underline{L}\rangle + a_8|d^8\underline{L}^2\rangle$ and $|\Phi_f\rangle = a_5'|d^5\rangle + a_6'|d^6\underline{L}\rangle + a_7'|d^7\underline{L}^2\rangle$. Adjustable parameters here are the d-d Coulomb interaction U, the p-to-d charge-transfer energy Δ, and the transfer integral $(pd\sigma)$. Racah parameters B and C have been fixed at 0.131 and 0.484, respectively.[38]

In order to estimate U and Δ, we refer to the parameters of $Cd_{1-x}Fe_xSe$ for the first step because the Fe $3d$-derived spectra of $Cd_{1-x}Fe_xSe$ are well explained by CI calculations for a tetrahedral $(FeSe_4)^{6-}$ cluster: $\Delta=1.5$ eV, $U=4.5$ eV, and $(pd\sigma)=-1.1$ eV.[39] It should be noted that the spectra of $Cd_{1-x}Mn_xTe$ with tetrahedrally coordinated Mn and MnTe with octahedrally coordinated Mn are equally well fitted using almost the same U and Δ,[39] with $(pd\sigma)$ for MnTe being smaller than that for $Cd_{1-x}Mn_xTe$ following Harrison's law.[40]

Figure 10 shows the result of the cluster-model calculation using parameters $\Delta=2$ eV, $U=5$ eV, and $(pd\sigma)$

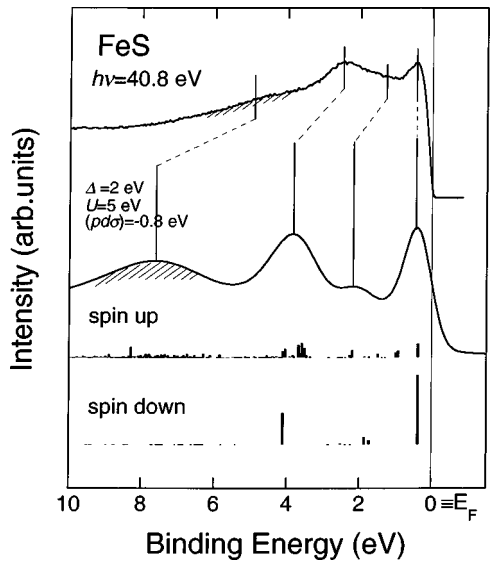

FIG. 10. Configuration-interaction cluster-model calculation for FeS compared with the observed spectrum. Vertical bars show the calculated energy positions and spectral weight.

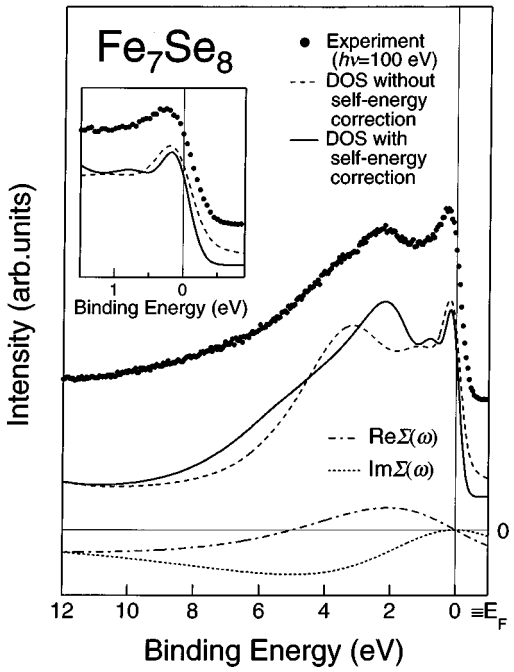

FIG. 11. Spectral DOS $\rho(\omega)$ of Fe_7Se_8 obtained by applying the self-energy correction to the band DOS of Ref. 24. The inset shows the spectra near the Fermi level. The real and imaginary parts of the model self-energy $\Sigma(\omega)$ are also shown.

$=-0.8$ eV, which are also close to values expected from chemical trends.[35] The obtained value $U=5$ eV is close to the value ($U\sim 4$ eV) estimated in Sec. IV A. Since $U>\Delta$, FeS is in the charge-transfer regime of the Zaanen-Sawatzky-Allen diagram.[41] The obtained transfer integral $(pd\sigma)$ is smaller than that in $Cd_{1-x}Fe_xSe$ due to the larger Fe-S distance in FeS. In the calculated spectrum, one can see four peaks at $E_B\sim 0.3$, 2, 4, and 6–10 eV. The structure at $E_B\sim 0.3$ eV mainly consists of $d^6\underline{L}$ states. The broad peak extending from $E_B\sim$ 6 to 10 eV consists of a mixture of d^5 and $d^7\underline{L}^2$ states, which should correspond to the satellite as shown in Fig. 3. The cluster-model calculation suggests the existence of a satellite at $E_B\sim 8$ eV. However, Fig. 10 shows that the agreement between the observed spectrum and the calculated spectrum is not satisfactory in the intensity of the satellite and the line shape of the main bands. Thus, even though electron correlation is important for the opening of the band gap in FeS and for the appearance of the high-binding-energy satellites, the spectral line shape of the main band is better described by the band-structure calculation.

D. Self-energy correction

Now we consider Fe_7Se_8 starting from the itinerant-electron limit and treat electron correlation as a self-energy correction. Instead of calculating the self-energy $\Sigma(\mathbf{k},\omega)$ theoretically using, e.g., perturbation theory,[42] we take an empirical approach. Namely, we assume a simple analytical form for ω-dependent but momentum-independent $\Sigma(\omega)$ and adjust parameters so as to reproduce the experimental spectra.[43] $\Sigma(\omega)$ has to satisfy several conditions: In the metallic states, the lifetime of a quasiparticle near E_F should be proportional to the square of energy from E_F: $\mathrm{Im}\Sigma(\omega)\propto\omega^2$.[44] Near E_F, $\mathrm{Re}\Sigma(\omega)$ should be linear in the binding energy. In order to satisfy these conditions, we have assumed a simple analytical form for $\Sigma(\omega)$, $\Sigma(\omega)=g\omega/(\omega+i\Gamma)^2$, where g and Γ are treated as adjustable parameters. The single-particle spectral DOS, $\rho(\omega)$, is thus given by

$$\rho(\omega)=-\frac{1}{\pi}\sum_k \mathrm{Im}\frac{1}{\omega-\omega_k^0-\Sigma(\omega)}$$
$$=-\frac{1}{\pi}\int d\epsilon N_b(\epsilon)\mathrm{Im}\frac{1}{\omega-\epsilon-\Sigma(\omega)}, \qquad (1)$$

where $N_b(\epsilon)$ is the Fe $3d$ partial DOS from the band-structure calculation.

As shown in Fig. 11, the overall line shape of the photoemission spectrum of Fe_7Se_8 is explained very well by the band DOS corrected for the self-energy with $g=17$ and $\Gamma=5$: The narrowing of the overall Fe $3d$ bandwidth and the appearance of the high-binding-energy tail have been well reproduced, indicating that the itinerant model gives a good starting point. (We have not attempted the self-energy analysis of the spectra of FeS starting from the LSDA DOS because the magnetic moment has not been reproduced by the LSDA calculation.) The mass enhancement factor m^*/m_b is given by $z^{-1}\equiv 1-\partial\mathrm{Re}\Sigma(\omega)/\partial\omega|_{\omega=0}=1+g/\Gamma^2$. Using the above g and Γ values, we obtain $m^*/m_b\sim 1.7$, where m_b and m^* are the bare band mass and the enhanced effective mass at E_F, respectively. This value is in the same range as the experimental values deduced from the electronic specific heats, $m^*/m_b\sim 2.6$ (Ref. 26) and ~ 1.4 (Ref. 27).

However, the above model self-energy $\Sigma(\omega)$ cannot explain the broadening of the peak near E_F as shown in the inset of Fig. 11 because z^{-1} cannot be smaller than unity and the self-energy correction narrows the bandwidth. Improvement of the self-energy correction by the inclusion of nonlocal effect,[45–47] i.e., the momentum dependence of the self-energy, is certainly necessary for further analyses. It should be noted that from the knowledge of the interacting electron gas with the Hartree-Fock approximation, the spectral inten-

sity near the Fermi level is lowered due to the momentum dependence of the self-energy, i.e., the exchange energy. Also, in order to explain the stronger discrepancy of the minority-spin spectrum between the band DOS and experiment than the majority-spin spectrum, the spin dependence of the self-energy correction will also have to be considered.

V. CONCLUSION

The electronic structures of FeS, Fe_7S_8, and Fe_7Se_8 have been studied using photoemission and inverse-photoemission spectroscopy. The resonant photoemission measurements show enhancement in the higher-binding-energy region, suggesting the existence of satellites. It is indicated that the localized nature of the $3d$ electrons in FeS is relatively strong and that of Fe_7Se_8 is relatively weak, with Fe_7S_8 being located intermediate between the two compounds.

Spectral weight redistribution in the valence band in going from FeS to Fe_7S_8 has been discussed based on both the itinerant band picture and the hole-doped Mott insulator picture. In order to understand the ground state of FeS in more detail, a band-structure calculation on the real (distorted NiAs-type) structure is desirable. We have compared the observed spectra with the calculated band DOS from the band-structure calculations. The observed overall Fe $3d$ bandwidths of Fe_7S_8 and Fe_7Se_8 are narrower and at high-binding-energies have stronger intensity than the band DOS. On the other hand, the peaks just below and above E_F are broadened compared with the band DOS. According to the SRPES measurements, the deviation of the measured spectra from the band DOS is stronger for the minority-spin band, suggesting a spin-dependent correlation effect. Although the CI cluster-model calculation for FeS yields a satellite, which may correspond to the high-binding-energy tail of the photoemission spectra, the overall agreement between experiment and theory is not satisfactory. Alternatively we have made a self-energy correction to the band DOS by introducing a model ω-dependent self-energy. The discrepancy between the band DOS and the observed spectrum of Fe_7Se_8 is considerably reduced, showing the validity of the itinerant band model for Fe_7Se_8 as a starting point as well as the importance of correlation effects. In spite of the overall agreement between the self-energy-corrected DOS and the photoemission spectra, serious discrepancies remain for the spectra near E_F. Nonlocal (i.e., momentum-dependent) and spin-dependent effects in the self-energy correction would have to be included in future studies.

ACKNOWLEDGMENTS

We would like to thank the staff of Synchrotron Radiation Laboratory for technical support. We also thank Professor Y. Murakami for help in the SQUID measurements. This work was supported by a Grant-in-Aid for Scientific Research from the Ministry of Education, Science and Culture, Japan.

*Present address: Hiroshima Synchrotron Radiation Center, Hiroshima University, Higashi-Hiroshima 739, Japan.

†Present address: Department of Applied Chemistry, University of Tokyo, Tokyo 113, Japan.

[1] K. Adachi, J. Phys. Soc. Jpn. **16**, 2187 (1961).

[2] M. G. Townsend, J. R. Gosselin, R. J. Tremblay, and A. H. Webster, J. Phys. (Paris) Colloq. **37**, C4-11 (1976).

[3] J. R. Gosselin, M. G. Townsend, and R. J. Tremblay, Solid State Commun. **19**, 799 (1976).

[4] E. F. Bertaut, J. Phys. Radium **15**, 77S (1954).

[5] A. F. Andresen, Acta Chem. Scand. **14**, 919 (1960).

[6] E. F. Bertaut, Acta Crystallogr. **6**, 557 (1953).

[7] A. Okazaki and K. Hirakawa, J. Phys. Soc. Jpn. **11**, 930 (1956).

[8] A. Okazaki, J. Phys. Soc. Jpn. **14**, 112 (1959).

[9] A. Okazaki, J. Phys. Soc. Jpn. **16**, 1162 (1961).

[10] K. Hirakawa, J. Phys. Soc. Jpn. **12**, 929 (1957).

[11] T. Kamimura, K. Kamigaki, T. Hirone, and K. Sato, J. Phys. Soc. Jpn. **22**, 1235 (1967).

[12] T. Kamimura, J. Phys. Soc. Jpn. **43**, 1594 (1977).

[13] M. Kawaminami and A. Okazaki, J. Phys. Soc. Jpn. **22**, 924 (1967).

[14] G. Fillion, J. L. Mattei, P. Rochette, and P. Wolfers, J. Magn. Magn. Mater. **104-107**, 1985 (1992).

[15] A. F. Andresen and J. Leciejewicz, J. Phys. (France) **25**, 574 (1984).

[16] M. Kawaminami and A. Okazaki, J. Phys. Soc. Jpn. **29**, 649 (1970).

[17] L. M. Levinson and D. Treves, J. Phys. Chem. Solids **29**, 2227 (1968).

[18] C. Boumford and A. H. Morrish, Phys. Status Solidi A **22**, 435 (1974).

[19] H. N. Ok and S. W. Lee, Phys. Rev. B **8**, 4267 (1973).

[20] H. N. Ok, K. S. Baek, and E. C. Kim, Solid State Commun. **87**, 1169 (1993); H. N. Ok, K. S. Baek, E. C. Kim, and C. S. Kim, Phys. Rev. B **48**, 3212 (1993); H. N. Ok, K. S. Baek, and E. B. Park, Solid State Commun. **92**, 459 (1994).

[21] M. Sato, T. Kamimura, and T. Iwata, J. Appl. Phys. **57**, 3244 (1985).

[22] H. Ikeda, M. Shirai, N. Suzuki, and K. Motizuki, Jpn. J. Appl. Phys., Suppl. **32-3**, 301 (1993).

[23] M. Shirai, N. Suzuki, and K. Motizuki, J. Electron Spectrosc. Relat. Phenom. **78**, 95 (1996).

[24] H. Ikeda, M. Shirai, N. Suzuki, and K. Motizuki, J. Magn. Magn. Mater. **140-144**, 159 (1995).

[25] K. Sato, H. Kida, M. Fujisawa, and T. Kamimura, J. Phys. (Paris) Colloq. **49**, C8-37 (1988).

[26] J. Serre, P. Gibart, and J. Bonnerot, J. Phys. (France) **30**, 93 (1969).

[27] H. Kobayashi, T. Nozue, T. Matsumura, M. Sato, T. Suzuki, and T. Kamimura (unpublished).

[28] A. Kakizaki, H. Ohkuma, T. Kinoshita, A. Harasawa, and T. Ishii, Rev. Sci. Instrum. **63**, 367 (1992).

[29] J. Fujii, T. Kinoshita, K. Shimada, T. Ikoma, A. Kakizaki, T. Ishii, H. Fukutani, A. Fujimori, K. Soda, and H. Sugawara, in *Proceedings of the International Workshop on Polarized Electron Sources and Electron Spin Polarimeters, Nagoya* (Universal Academy Press, Tokyo, 1992).

[30] R. Denecke, L. Ley, and J. Fraxedas, Phys. Rev. B **47**, 13 197 (1993).

[31] Y. Ueda, M. Taniguchi, T. Mizokawa, A. Fujimori, I. Souma, and Y. Oka, Phys. Rev. B **49**, 2167 (1994).

[32] J. J. Yeh and I. Lindau, At. Data Nucl. Data Tables **32**, 1 (1985).

[33] U. Fano, Phys. Rev. **124**, 1866 (1961).
[34] A. Liebsch, Phys. Rev. Lett. **43**, 1431 (1979); L. C. Davis and L. A. Feldkamp, J. Appl. Phys. **50**, 1944 (1979).
[35] A. E. Bocquet, T. Mizokawa, T. Saitoh, H. Namatame, and A. Fujimori, Phys. Rev. B **46**, 3771 (1992).
[36] A. E. Bocquet, T. Saitoh, T. Mizokawa, and A. Fujimori, Solid State Commun. **83**, 11 (1992).
[37] A. Fujimori, F. Minami, and S. Sugano, Phys. Rev. B **29**, 5225 (1984); A. Fujimori and F. Minami, *ibid.* **30**, 957 (1984).
[38] Y. Tanabe and S. Sugano, J. Phys. Soc. Jpn. **9**, 766 (1954).
[39] T. Mizokawa and A. Fujimori, Phys. Rev. B **48**, 14 150 (1993).
[40] W. A. Harrison, *Electronic Structure and the Properties of Solids* (Dover, New York, 1989).
[41] J. Zaanen, G. A. Sawatzky, and J. W. Allen, Phys. Rev. Lett. **55**, 418 (1985).
[42] G. Tréglia, F. Ducastelle, and D. Spanjaard, J. Phys. (France) **43**, 341 (1982).
[43] T. Saitoh, A. Sekiyama, T. Mizokawa, A. Fujimori, K. Ito, H. Nakamura, and M. Shiga, Solid State Commun. **95**, 307 (1995).
[44] A. Kawabata, Physica B **86-88**, 387 (1977).
[45] S. Massida, M. Posternak, and A. Baldereschi, Phys. Rev. B **46**, 11 705 (1992).
[46] J.-Y. Son, T. Konishi, T. Mizokawa, A. Fujimori, K. Koui, and T. Goto, Physica B **237-238**, 400 (1997).
[47] I. H. Inoue, I. Hase, Y. Aiura, A. Fujimori, Y. Haruyama, T. Maruyama, and Y. Nishihara, Phys. Rev. Lett. **74**, 2539 (1995).